

Received March 7, 2020, accepted March 24, 2020, date of publication March 31, 2020, date of current version April 17, 2020.

Digital Object Identifier 10.1109/ACCESS.2020.2984530

A Circumferential Coupled Dipole-Coil Magnetic Coupler for Autonomous Underwater Vehicles Wireless Charging Applications

CHUNWEI CAI^{1,2}, (Member, IEEE), YANYU ZHANG¹, SHUAI WU¹, JINQUAN LIU¹, ZHIPENG ZHANG¹, AND LONGYUN JIANG¹

¹School of New Energy, Harbin Institute of Technology, Weihai 264209, China

²Shandong Institute of Shipbuilding Technology, Weihai 264209, China

Corresponding author: Chunwei Cai (caichunwei@hit.edu.cn)

This work was supported in part by the Natural Science Foundation of Shandong Province of China under Grant ZR2019MEE052, and in part by the Major Scientific and Technological Innovation Project of Shandong Province of China under Grant 2017CXGC0921.

ABSTRACT Inductive power transfer is a practical approach to recharging the autonomous underwater vehicles (AUVs). The performance of the magnetic coupler determines the system transfer capacity. The annular magnetic coupler is widely utilized in the underwater wireless charging system. However, this magnetic coupler has limitations on magnetic field distribution. The flux linkage occupies the center of the AUV, and hence, the electronics inside the AUV are susceptible to electromagnetic interference. Additionally, the weight of the annular magnetic coupler greatly increases the burden on AUV power supply. In this paper, the magnetic coupler structure evolution is analyzed and a dipole-coil-based magnetic coupler with a novel circumferential coupling manner is presented. The magnetic flux is perfectly confined by the coupling manner, and the magnetic coupler weight is reduced by dimension optimization. To implement the magnetic coupler, the Fe-based nanocrystalline soft magnetic material is taken into consideration. To validate the proposal, a wireless charging system is built. Experimental results show that the system transfers 630W under water with a DC-DC efficiency of 89.7%.

INDEX TERMS Autonomous underwater vehicles (AUVs), inductive power transfer (IPT), magnetic coupler design, coupling manner.

I. INTRODUCTION

Wireless power transfer is known by Tesla's experiment in 1890 [1]. Nowadays, wireless power transfer technology is widely used in electronics [2], [3], biomedical implants [4], [5] and electric vehicles [6], [7]. The AUV is an important underwater equipment for exploring the marine ecological environment, to provide a favorable means for gathering marine information [8]. However, the capacity of rechargeable batteries carried by the AUV is limited, which cannot sustain sufficiently mission times [9]. Swapping batteries need manual intervention, and establishing a wired charging station under water requires perfect air tightness [10]. The inductive power transfer system for the underwater sensors of ocean buoys has been proposed in [11], [12]. To charge the

The associate editor coordinating the review of this manuscript and approving it for publication was F. R. Islam.

AUV under water safely and conveniently, Feezor *et al.* took advantage of wireless charging technology and proposed an inductive interface to supply power to AUV [13].

The magnetic coupler in a wireless power transfer system are of great importance, as they determine the power transfer performance and the magnetic field distribution. He *et al.* proposed a three-dimensional omnidirectional underwater wireless power transfer system. However, the coil structure is hard to implement on AUV wireless charging [14]. Zhou *et al.* proposed a PM-type magnetic coupler, which transfers 300W under water at a DC-DC efficiency of 85% [9]. Cheng *et al.* investigated the additional eddy current loss in various water media and proposed a semi-closed magnetic coupler which transfers 10kW at 91% [15]. However, neither the PM-type magnetic coupler nor the semi-closed magnetic coupler has taken the compatibility with the AUV's hull into consideration. To install the magnetic

coupler, additional fixtures are required to be installed on the AUV surface, which may destroy AUV's streamlined structure and increase AUV march friction. To match the AUV's hull, Wang *et al.* designed an annular magnetic coupler and a miniature prototype was produced to verify the proposal [16]. However, the weight of the annular ferrite core is a great burden on the AUV power supply, since large amounts of ferrite need to be used. Additionally, the annular ferrite core is very difficult to sinter. Lin *et al.* designed a pair of coaxial and coreless coil structure, which was installed on the AUV's head, and the coupling coefficient k reaches 0.8 [9]. Nevertheless, the annular magnetic coupler and coreless coil structure both need a large gap over 15mm between the AUV and the docking station. For a narrow air gap, it is almost impossible for AUV to enter the docking station conveniently. Moreover, these magnetic couplers ignore the magnetic field distribution, which may lead to the equipment in AUV affected by electromagnetic interference. Tianze Kan *et al.* studied the annular magnetic coupler magnetic field distribution and proposed a three-phase system with several segmented ferrite bars and the ferrite cores were installed in the AUV [17], [18]. However, the installation of ferrite bars is inappropriate, which may occupy more space in the AUV compartment. Yan *et al.* [19] proposed an arc-shaped magnetic coupler so that it is not necessary to change the shape of the AUV. Moreover, the transmission efficiency with the effect of eddy current is analyzed by the finite element method. The arc-shaped magnetic coupler is based on EE structure and the magnetic core need to be changed to match the AUV's hull, which brings the problem of ferrite material manufacture. In [20], [21], a curly coil structure is proposed for AUV underwater charging. The unipolar or bipolar coils is attached to the inner surface of AUV. By analyzing the magnetic field distribution, a larger aluminum plate is needed to shield electromagnetic interference in AUV. Therefore, designing a lightweight magnetic coupler with a well-confined magnetic field distribution is a problem to be solved.

To design a lightweight and well-coupled magnetic coupler with the internal electronics free from the electromagnetic interference caused by the flux linkage, in this paper, the coupling manner of the magnetic coupler is analyzed. The circumferential coupling manner possesses a low magnetic flux density at the center of the AUV verified by simulation models in ANSYS Maxwell. To implement the circumferential coupling manner, a dipole-coil-based magnetic coupler is proposed and the coupler dimension is designed to meet the misalignment requirement. Meanwhile, the weight and the air gap are optimized. Out of consideration for the magnetic coupler application, Fe-based nanocrystalline soft magnetic material is used as an alternative to ferrite materials. And, the coupling coefficient (k) and mutual inductance (M) are compared with the ferrite material under misalignments. Finally, a prototype is established to verify the proposal.

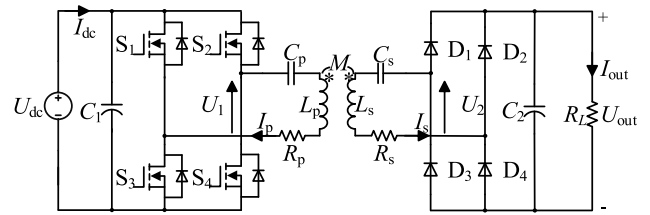


FIGURE 1. The wireless power transfer system with SS compensation.

II. WIRELESS POWER TRANSFER SYSTEM

In a wireless power transfer system, the k and M are important parameters for evaluating the magnetic coupler, as they reflect the coupling state and power transmission capability.

To get the relationship between the output power and M , a wireless power transfer system with SS compensation is built in Fig. 1. U_{dc} is the dc input voltage, and an H-bridge inverter, composed of four full-controlled switches S_1 - S_4 , is used to generate a high frequency ac power. A compensation capacitance C_p is chosen so that its impedance is matched to the primary side inductance L_p at the operating frequency. This also contributes the current I_p in L_p to resonating and generating a high magnetic flux density near L_p . Most of the magnetic flux passes through the receiver coil. The compensation network minimizes the VA rating of the power supply for a given load because the switches only pass real power. Additionally, a series compensation capacitance C_s is chosen to match the secondary side inductance L_s at the operating frequency. R_p and R_s are the parasitic resistance of L_p and L_s respectively. The rectifier consists of four diodes D_1 - D_4 . U_{out} and I_{out} are the voltage and current on load R_L separately.

U_1 and U_2 are the fundamental root-mean-square (RMS) values of ac voltage. By the Fourier decomposition of the square wave, U_1 and U_2 are shown in (1).

$$\begin{cases} U_1 = \frac{2\sqrt{2}}{\pi} U_{dc} \\ U_2 = \frac{2\sqrt{2}}{\pi} U_{out} \end{cases} \quad (1)$$

Based on Kirchhoff's voltage law, equation (2) can be obtained.

$$\begin{cases} \dot{U}_1 = \dot{I}_p(R_p + j\omega L_p + \frac{1}{j\omega C_p}) + j\omega M \dot{I}_s \\ \dot{U}_2 = \dot{I}_s(R_s + j\omega L_s + \frac{1}{j\omega C_s}) + j\omega M \dot{I}_p \end{cases} \quad (2)$$

where ω is the operating angular frequency. When ω is equal to the resonance angular frequency, equation (2) can be simplified and written as

$$\begin{cases} \dot{U}_1 = \dot{I}_p R_p + j\omega M \dot{I}_s \\ \dot{U}_2 = \dot{I}_s R_s + j\omega M \dot{I}_p \end{cases} \quad (3)$$

Therefore, the current in the primary coil and secondary coil are expressed as

$$\begin{cases} \dot{i}_p = \dot{U}_2 \frac{-j\omega M + R_s \dot{U}_1}{R_p R_s + (\omega M)^2} \\ \dot{i}_s = \dot{U}_1 \frac{-j\omega M + R_p \dot{U}_2}{R_p R_s + (\omega M)^2} \end{cases} \quad (4)$$

Considering the utilize of litz wire, the parasitic resistance R_p and R_s can be ignored. As a result, the simplified expression is shown in (5).

$$\begin{cases} \dot{i}_p = \frac{\dot{U}_2}{j\omega M} \\ \dot{i}_s = \frac{\dot{U}_1}{j\omega M} \end{cases} \quad (5)$$

By substituting (1) into (5), the RMS values of I_p and I_s can be solved as

$$\begin{cases} I_p = \frac{2\sqrt{2} U_{out}}{\pi \omega M} \\ I_s = \frac{2\sqrt{2} U_{dc}}{\pi \omega M} \end{cases} \quad (6)$$

The current I_{out} and output power P_{out} can be written as

$$I_{out} = \frac{2\sqrt{2} I_s}{\pi} = \frac{8 U_{dc}}{\pi^2 \omega M} \quad (7)$$

$$P_{out} = I_{out}^2 R_L = \frac{64 U_{dc}^2}{\pi^4 \omega^2 M^2} R_L \quad (8)$$

As shown in (6), (7) and (8), the M is a greatly important parameter for the wireless charging system, as the M has a directly influence on I_p , I_s , I_{out} and P_{out} . To achieve the required output power, the M should satisfy (8).

In the wireless power transfer system, the $k = M/\sqrt{L_p L_s}$ and equation (8) can be written as

$$P_{out} = I_{out}^2 R_L = \frac{64 U_{dc}^2}{\pi^4 \omega k^2 L_p Q_2} \quad (9)$$

where Q_2 is the load-dependent quality factor for secondary side and $Q_2 = \omega L_s/R_L$.

Despite the output power and current are closely related to M , for different magnetic coupler structures, the k provides a useful measure for directly comparing magnetic properties of different magnetic couplers.

In general, compared to the k over 0.95 in conventional transformer, the wireless power transfer system has a typical value between 0.01 and 0.8. High values are desired because less magnetomotive force is required to get the same power-level transfer. However, the higher the k is, the higher the sensitivity of the magnetic coupler to misalignment will be, which may result in power fluctuation during the charging of AUV. For the underwater environment, misalignments always occur when the AUV is homing to the docking station. The axial misalignment is limited within 30mm [22] and the maximum rotational misalignment is 10° . To obtain a good coupling effect and stable power transmission, a trade-off between high k and low sensitivity is necessary.

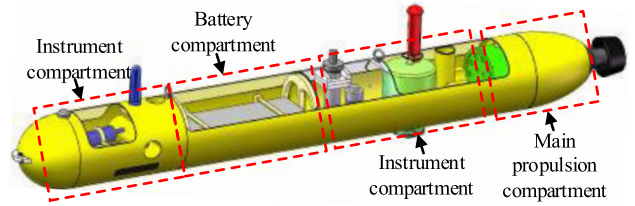


FIGURE 2. AUV overview.

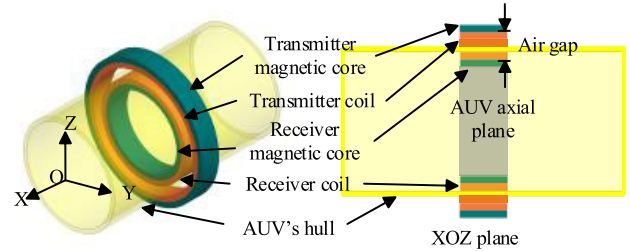


FIGURE 3. Annular magnetic coupler and installation.

III. COUPLING LIMITS OF ANNULAR MAGNETIC COUPLER

Fig. 2 shows the AUV with an outer diameter of 300mm and a bulkhead thickness of 4mm. The charging system including a 500-mm-length 200-mm-wide and 180-mm-height lithium battery is placed in the battery compartment.

To charge the AUV underwater, the annular magnetic coupler is widely used in the wireless charging system. An annular magnetic coupler simulation model is established in ANSYS Maxwell and shown in Fig. 3, the air gap between the transmitter and receiver is indispensable. For a 300mm outer diameter AUV, the internal diameter of the docking station should be larger than 330mm. The transmitter is fixed on the docking station, however, to sinter a 330mm diameter annular magnetic core is extremely difficult for the current manufacturing technology. Additionally, the heavier the magnetic core is, the higher the power used to generate the propulsion is.

As shown in Fig. 4, the magnetic flux of the annular magnetic coupler is distributed on the AUV's XOZ plane and the flux linkage is mainly divided into leakages flux (Φ_1) and mutual flux (Φ_2). As can be seen, the primary coil and secondary coil are coupled with Φ_2 . The flux linkage is extended along the AUV's axis and coupled in the AUV. The battery compartment is covered by flux linkage.

Furthermore, due to the compact space limit, the internal electronics are susceptible to electromagnetic interference. To evaluate the magnetic flux density in the vicinity of AUV, a 3D simulation magnetic field in the XOZ plane is shown in Fig. 5.

According to the International Commission on Non-Ionizing Radiation Protection (ICNRP) guidelines, the magnetic flux density minimum is set to $20\mu T$ [23]. Although Fig. 5 shows that the magnetic flux is mainly converged in the edge of the hull, the magnetic flux density in the

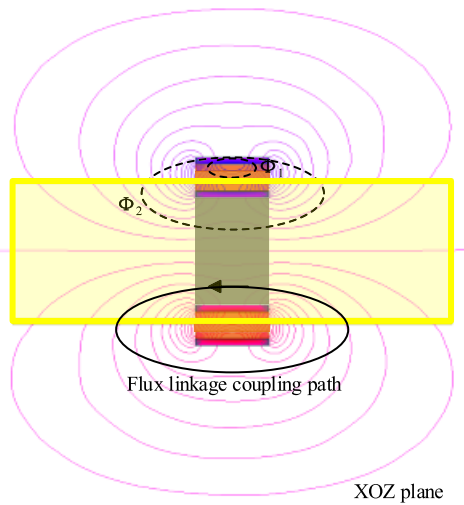


FIGURE 4. Annular magnetic coupler and axial coupled flux linkage.

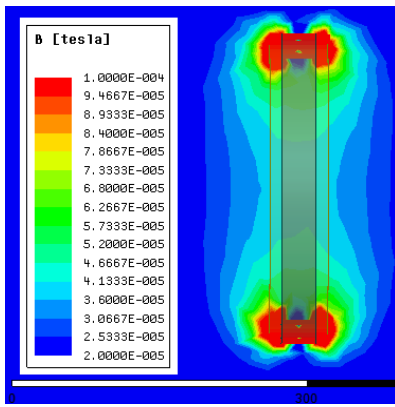


FIGURE 5. Magnetic flux density in the XOZ plane.

center of AUV is obviously higher than $20\mu\text{T}$. The AUV is surrounded by magnetic field, which may limit the internal electronics layout. The distribution result indicates that the coupled flux linkage fails to keep the magnetic flux away from the electronics.

In summary, the requirements imposed on the magnetic coupler for AUV underwater wireless charging are as follows:

- 1) The magnetic coupler satisfies the battery compartment space limits, and avoids the high-density magnetic field generated inside the AUV.
- 2) The k reaches 0.4 and when the magnetic coupler is misaligned, the variation is less than 0.1.
- 3) The magnetic core should be lightweight and easy to be implemented in the application.

IV. NOVEL MAGNETIC COUPLER DESIGN

A. MAGNETIC COUPLER PROPOSED

The coupling limits on annular magnetic coupler have been described in section III. Actually, the annular magnetic coupler is a two-layer solenoid. As shown in Fig.6, the inner solenoid is wrapped by the outer solenoid, and hence the

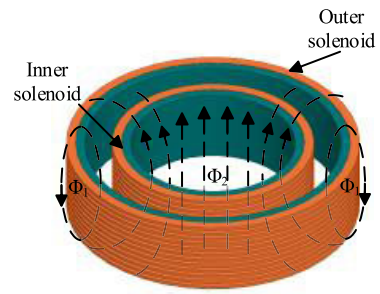
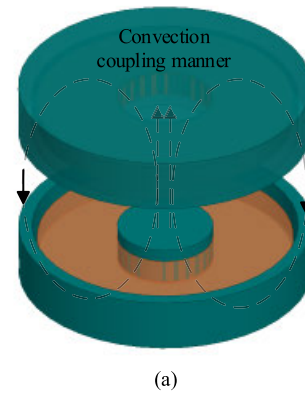
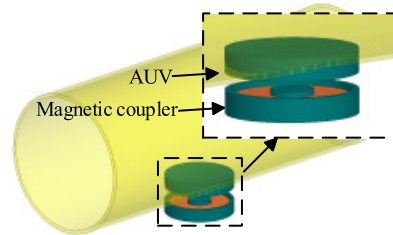


FIGURE 6. Two-layer solenoid structure and coupling manner.



(a)



(b)

FIGURE 7. Pot-type magnetic coupler (a) pot-type magnetic coupler and coupling manner. (b) pot-type magnetic coupler installation on AUV.

flux linkage extends along the solenoid height and forms a closed loop.

Fig. 7 shows a pot-type magnetic coupler whose coupling manner is similar to the conventional transformer. The pot-type magnetic coupler can be regarded as the inner solenoid being taken out and placed on the outer solenoid. Therefore, the flux linkage in Fig. 7(a) is coupled like the atmosphere convection and closed along the magnetic coupler edge. The magnetic field area is mainly concentrated in the magnetic coupler, which implements a well-confined magnetic field distribution. However, the pot-type structure flux linkage is perpendicular to the magnetic coupler which is more sensitive to axial and rotational misalignments. In addition, as shown in Fig. 7(b), the AUV's hull should be changed to install the magnetic coupler.

To meet the magnetic coupler requirements, a novel magnetic coupler structure need to be designed and the magnetic coupler structure and coupling manner should be considered.

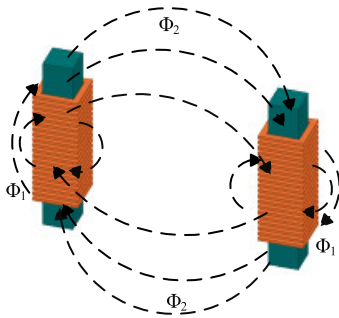


FIGURE 8. Magnetic dipoles structure and coupling manner.

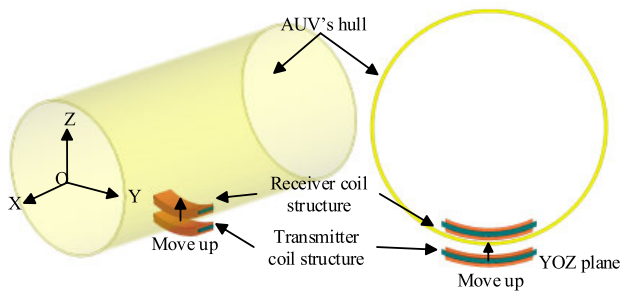


FIGURE 9. Dipole-coil-based magnetic coupler and installation.

The evolution from annular magnetic coupler to pot-type magnetic coupler indicates that both the magnetic field distribution and magnetic coupler weight are optimized. From the inner solenoid position point of view, when the primary and secondary magnetic core is separated, the magnetic coupler can be smaller and the magnetic field is constrained at the bottom of the AUV. Fig. 8 shows a magnetic coupler composed of two magnetic poles and the coupling manner is shown by the dotted line. The structure can be viewed as the inner solenoid being taken out and placed in parallel with the out solenoid. Compared to the annular magnetic coupler and pot-type magnetic coupler, the magnetic dipole structure separates the inner and outer solenoid completely, and hence, the magnetic coupler installation is more flexible.

According to the coupling manner in the annular magnetic coupler and the pot-type magnetic coupler, it is difficult to take the coupling manner, magnetic field distribution and magnetic coupler installation into consideration at the same time. As shown in Fig. 9, a dipole-coil-based magnetic coupler is applied to the AUV underwater wireless charging system and the receiver coil structure is fixed on the inner surface of AUV, which could match the AUV without changing the AUV's hull. The flux linkage is shown in Fig. 10. The novel magnetic coupler constrains the magnetic field in AUV circumferential direction. As can be seen, although the magnetic coupler structure determines the flux linkage cannot achieve an ideal utilization rate, most of the mutual flux Φ_2 passes through the secondary coil. The flux linkage is extended and coupled along the AUV's hull. Clearly, the height of the magnetic flux is limited lower than the secondary magnetic core.

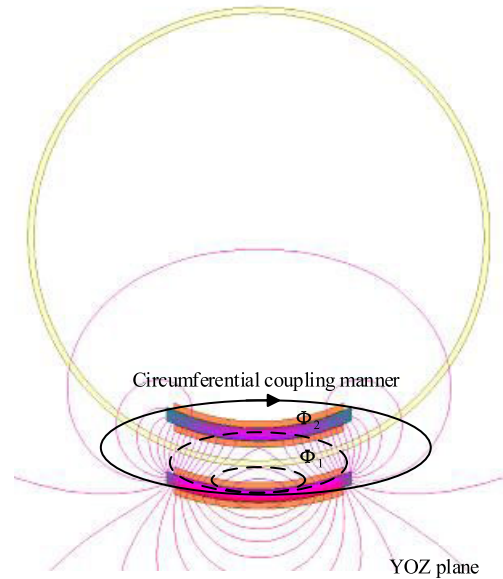


FIGURE 10. The proposed magnetic coupler with circumferential coupled flux linkage.

Additionally, the magnetic coupler can be pushed to approach the AUV. The air gap could be reduced to 8mm, considering the 4mm litz wire. The volume of the dipole-coil-based magnetic coupler is much smaller than the former two couplers, which indicates the weight of the novel magnetic coupler could be lighter and the AUV internal space will be saved. The novel magnetic coupler has a better effect not only in magnetic field distribution but also in reducing air gap and magnetic coupler weight.

B. MAGNETIC FIELD DENSITY STUDIES

To study the magnetic field density at the center of the AUV, both the annular magnetic coupler and the dipole-coil-based magnetic coupler are set to the same primary coil current RMS value 10A. The two magnetic couplers are implemented in ANSYS Maxwell, and the results of the magnetic flux density of the two magnetic couplers in YOZ, XOZ, and XOY plane are shown in Figs. 11-13, respectively. Taking the ICNIRP guidelines and the magnetic field in the AUV into consideration, the minimum density of the magnetic field is set to $20\mu\text{T}$ and the maximum value is $100\mu\text{T}$.

Fig. 11(a) indicates the dipole-coil-based magnetic coupler has an outstanding performance on the magnetic field. In particular, the electronics are placed in the dashed box area. As can be seen from the scale bar, the flux density of the novel magnetic coupler is less than $20\mu\text{T}$ in the dashed box whereas the annular magnetic coupler is evidently higher than $40\mu\text{T}$.

Fig. 12 and Fig. 13 show the length and width of the magnetic field in the XOZ and XOY planes. Owing to the coupling manner in the dipole-coil-based magnetic coupler, the length and width of the magnetic field are mainly determined by the magnetic coupler dimension. Consequently, the magnetic field distribution is near the magnetic core and

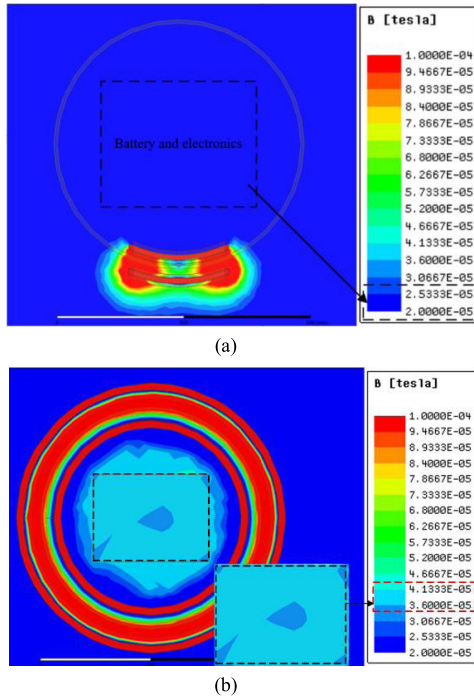


FIGURE 11. Magnetic flux density in the YOZ plane. (a) The dipole-coil-based magnetic coupler, (b) The annular coil structure.

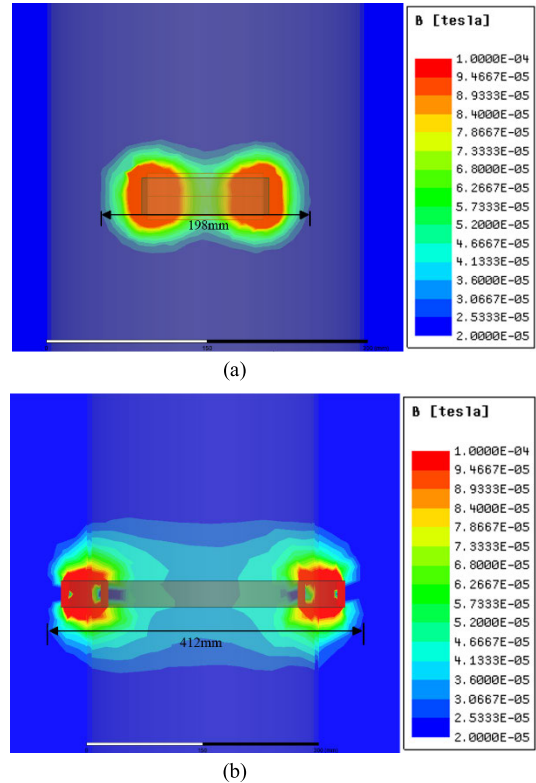


FIGURE 13. Magnetic flux density in the XOY plane. (a) The dipole-coil-based magnetic coupler, (b) The annular magnetic coupler.

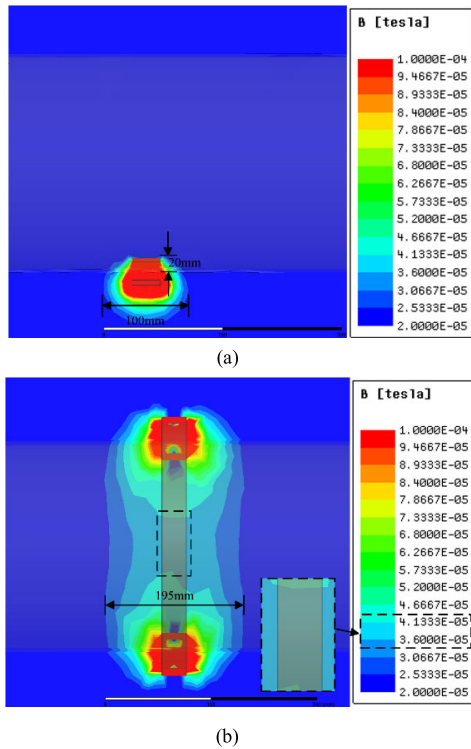


FIGURE 12. Magnetic flux density in the XOZ plane. (a) the dipole-coil-based magnetic coupler, (b) the annular magnetic coupler.

the flux height in the AUV is only 20mm. However, the axial coupled flux linkage in annular magnetic coupler extends longer than the annular magnetic coupler and has a width of 195mm. The Fig. 13(b) shows the battery compartment is

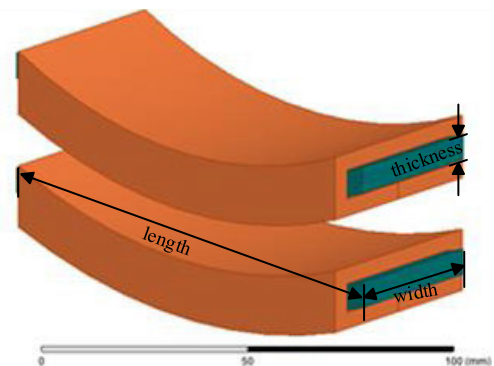


FIGURE 14. The dipole-coil-based magnetic coupler.

filled with a magnetic field, and the coverage area reaches 412mm × 195mm in the XOY plane.

C. DIPOLE-COIL-BASED MAGNETIC COUPLER DIMENSION OPTIMIZATION

To meet the requirements of the k , the magnetic coupler dimensions are optimized in ANSYS Maxwell. As shown in Fig. 14, since the dipole-coil-based magnetic coupler is compatible with the AUV, the optimized parameters include the length, width and thickness. Generally, the coupling effect under rotational and axial misalignment are mainly decided by the length and the width of the magnetic coupler. Therefore, the optimization process can be simplified.

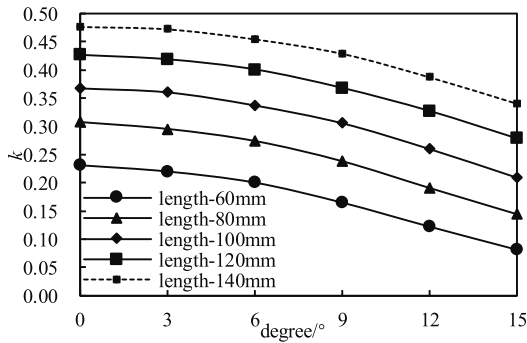


FIGURE 15. The variation of k with the length varying from 60mm to 120mm under rotational misalignments.

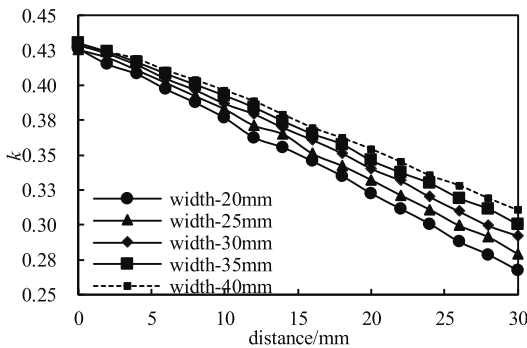


FIGURE 16. The variation of k with the width varying from 20mm to 40mm under axial misalignments.

The optimization dimension is based on the practical raw ferrite material and manufacture technology. The raw ferrite material dimension is 120mm × 35mm × 17mm. The length is set from 60mm to 140mm with the rotational angle from 0° to 15° and the width is from 20mm to 40mm with the axial misalignments from 0mm to 30mm. The variation of k is shown in Fig. 15 and Fig. 16.

Fig. 15 shows the variation of the k with different lengths. The variation shows the longer the dipole-coil-based magnetic coupler is, the higher the k is and when the simulated length is 140mm, the k reaches 0.48. The decline of k with different lengths is equal and the difference between the maximum and the minimum of k is 0.13, which indicates the initial value of the k is dependent on the length.

As shown in Fig. 16, when the width is increased from 20mm to 40mm, the difference between the maximum and the minimum is declined from 0.16 to 0.11. The initial k of different width is at 0.43. Contrary to the effect of length on the k , the decline trend of k is chiefly dependent on the width of the dipole-coil-based magnetic coupler.

Due to the limits on manufacture technology, the magnetic core thickness is required to less than 12mm. The thickness optimization is carried out from 6mm to 12mm, and the performance of k under axial misalignment is shown in Fig. 17. The novel coupling manner extends in the circumferential plane and most of the flux linkage are concentrated in the upper of the transmitter and the lower of the receiver. For different axial misalignments with the same thickness,

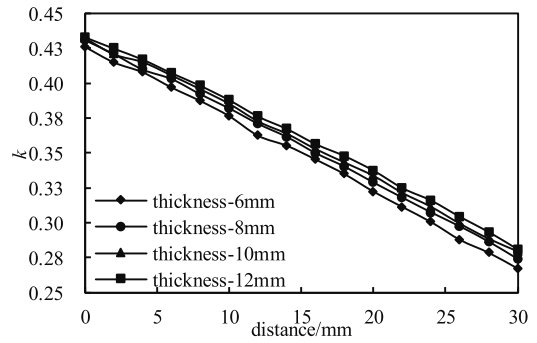


FIGURE 17. The variation of k with the thickness varying from 6mm to 12mm under axial misalignments.

TABLE 1. Magnetic properties dimension of dipole-coil-based magnetic coupler.

Parameters	Value
Air gap	8mm
Wire diameter	4mm
Magnetic core size	120mm×35mm×6mm
Transmitting coil turns N_p	20
Receiving coil turns N_s	20

the maximum variation of k is 0.01. Compared to the effect of width and length on misalignment, the thickness has less influence on k .

Combined with the raw material dimension and the requirements of k , the length and width are set to 120mm and 35mm, respectively. Meanwhile, the thickness is set to 6mm to reduce the weight. Ideally, according to calculation, the novel magnetic coupler weight is 252g and the annular magnetic is 1952g, which is seven times heavier than the novel coupler. The optimized dimensions of the dipole-coil-based magnetic coupler are shown in TABLE 1.

D. DIPOLE-COIL-BASED MAGNETIC COUPLER WITH NANOCRYSTALLINE SOFT MAGNETIC MATERIAL

Ferrite is widely utilized in the wireless power transfer system, but the ferrite is brittle. In this paper, the dipole-coil-based magnetic coupler requires an arc-shaped surface to match the AUV, which is much difficult for the ferrite material manufacturing technology. In the late 1980s, the saturation magnetic induction intensity, permeability and loss of Fe-based nanocrystalline soft magnetic materials are greatly improved. The Fe-based nanocrystalline soft magnetic material is superior to conventional materials, which are reflected in higher saturation magnetic flux density, higher relative permeability and less core loss. More importantly, the proposed magnetic coupler is easy to be obtained with nanocrystalline soft magnetic material. The parameters of Fe-based nanocrystalline material are shown in TABLE 2.

Considering the difficulty in practical application, this paper chooses the nanocrystalline soft magnetic material to implement the dipole-coil-based magnetic coupler. The nanocrystalline soft magnetic material has a high saturation

TABLE 2. Fe-based nanocrystalline material parameters.

Symbol	Parameters	Value
B_s	saturation magnetic induction	1.25T
μ_0	Initial permeability	$>10^5$
μ_{max}	Maximum magnetic permeability	$>60 \times 10^4$
P_{loss}	Core loss	$P_{20kHz/0.5T} < 10W$

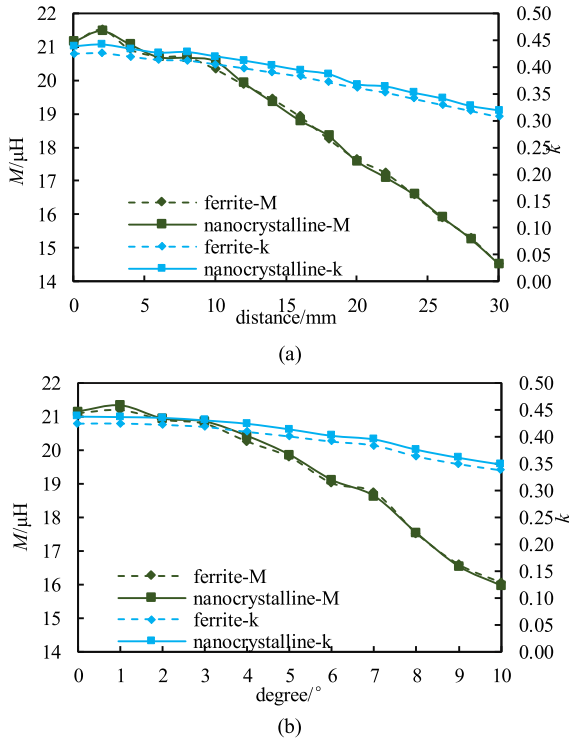


FIGURE 18. Comparison of the nanocrystalline material and ferrite under misalignments. (a) Variation of M and k with axial misalignments. (b) Variation of M and k with rotational misalignments.

magnetic induction B_s 1.25T. To verify that the dipole-coil-based magnetic coupler with Fe-based nanocrystalline material has the similar effect as the ferrite material, two magnetic material simulation models with the same dimensions are established. The variations of k and M are conducted under axial and rotational misalignments.

Misalignment simulation results are shown in Fig. 18. From simulation results, it can be seen that the properties of the two materials are similar, and the variation trends are consistent. On a whole, the k of Fe-based nanocrystalline soft magnetic material is slightly higher than that of ferrite material, with a maximum difference of 0.02. When aligned, the k of the Fe-based nanocrystalline soft magnetic material is 0.44 and the minimum is 0.32, which is 0.01 higher than that of the ferrite material. The M of the two materials are almost equal, and the maximum difference is less than $0.2 \mu H$. The M of Fe-based nanocrystalline soft magnetic material drops from $21.5 \mu H$ to $14.5 \mu H$. It can be seen from the simulation analysis results that the difference between the nanocrystalline material and ferrite is very small.

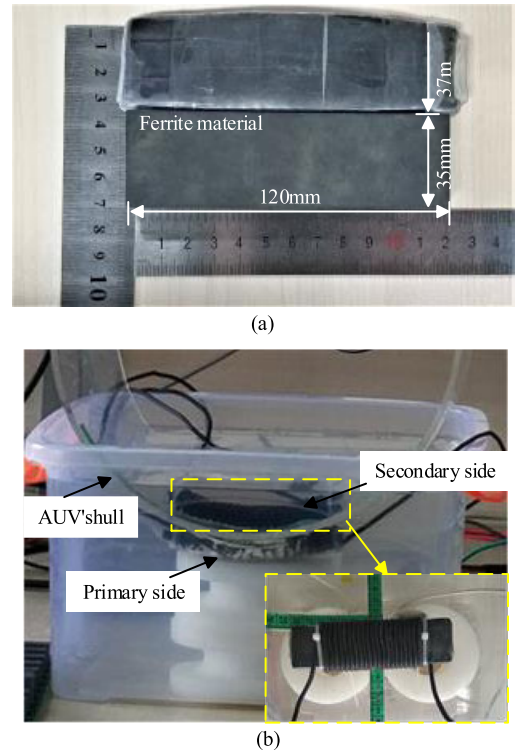


FIGURE 19. The prototype of the dipole-coil-based magnetic coupler. (a) Comparison with the raw ferrite material. (b) The dipole-coil-based magnetic coupler overview.

TABLE 3. Dipole-coil-based magnetic coupler parameters.

Parameters	Values
Air gap	8mm
Core size	125mm*37mm*8mm
Receiver	137g
Wire diameter	4mm
Number of turns in L_p	20
Number of turns in L_s	20

V. EXPERIMENT

Based on the simulation model, the Fe-based nanocrystalline soft magnetic coupler prototype and raw ferrite core are both shown in Fig. 19 a). Due to the waterproof materials on the surface, the nanocrystalline dimensions are a bit bigger than the raw ferrite material. However, the total weight of the magnetic coupler is 267.4g and the receiver is 137g, which can be ignored for the AUV power supply. The dimensional parameters of the magnetic coupler are given in TABLE 3. As shown in Fig. 19 b), the coil structure is placed in seawater. The M and k between the transmitter and the receiver are calculated during misalignments. The results compared with the simulations are shown in Fig. 20, which shows that measurements are well-matched to the simulations.

When the magnetic coupler is aligned, the k of simulated and measured results are 0.44 and 0.40, respectively. In the process of misalignment, the maximum difference between

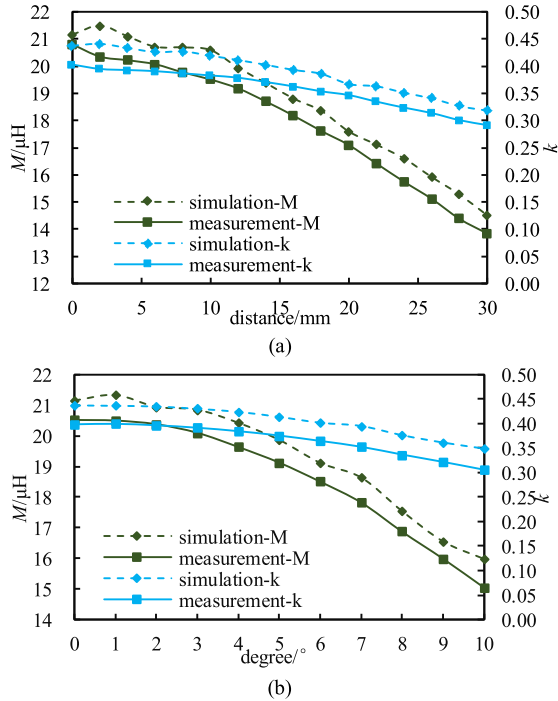


FIGURE 20. Comparison of the simulation and measurement under misalignments. (a) Variation of M and k with axial misalignments. (b) Variation of M and k with rotational misalignments.

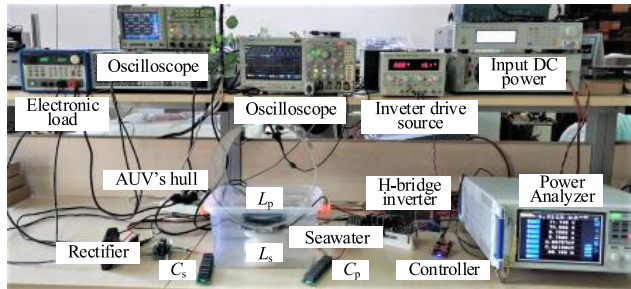


FIGURE 21. Wireless power transfer system prototype.

simulated and measured is less than 0.05. The measured k of the axial misalignment at 30mm is 0.29, and the k variation is 0.1, which satisfies the requirement. In the case of axial and rotational misalignment, the maximum difference of the measured and simulated M is $1.13\mu\text{H}$. The measured value of the M drops from $20.8\mu\text{H}$ to $13.9\mu\text{H}$, when the axial distance varies from 0mm to 30mm.

The wireless power transfer system prototype is built and shown in Fig. 21. The input DC voltage is fixed at 72V, and to transfer over 600Watts, the electronic load is set to 8Ω . In detail, the system parameters are shown in TABLE 4. The TI microcontroller TMS320F28027 is employed to generate 4 PWMs to drive the 4 SiC MOSFETs in the H-bridge inverter and the switching frequency is 50 kHz.

To alleviate the switching loss, copper loss, and core loss resulting from the high switching frequency, a larger C_p is chosen to achieve soft switching and litz wires are selected to minimize the skin effects. Moreover, C_s is a bit larger than the

TABLE 4. Experiment parameters.

Symbol	Parameters	Value
U_{dc}	Input DC voltage	72V
f	Operating frequency	50kHz
L_p	The primary self-inductance	51.46 μH
R_p	Parasitic resistance in transmitter coil	90.34m Ω
C_p	The primary compensation capacitance	220nF
L_s	The secondary self-inductance	52 μH
R_s	Parasitic resistance in receiver coil	92.4m Ω
C_s	The secondary compensation capacitance	220nF
R_L	Load resistance	8 Ω

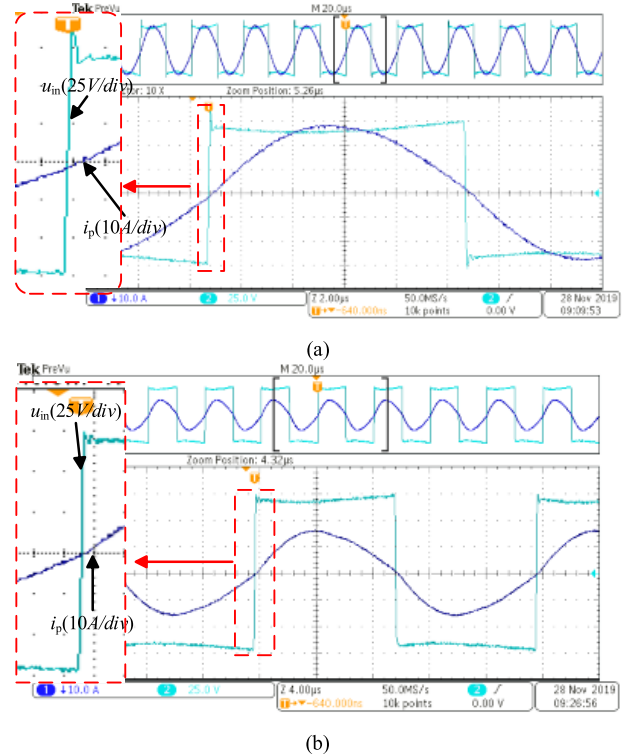
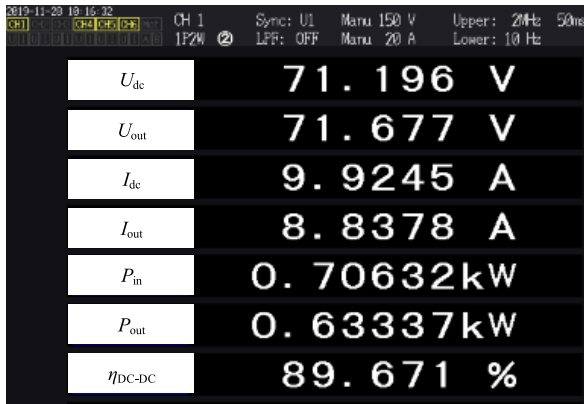


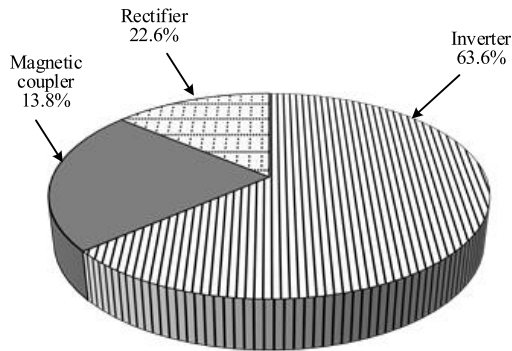
FIGURE 22. Measured waveforms of inverter voltage and current. (a) Waveforms measured at 0mm. (b) Waveforms measured at 30mm.

value calculated at resonance frequency 50kHz considering the misalignments. The waveforms measured at 0mm and 30mm are shown in Fig. 22, which indicates the system achieves soft switching when fully aligned and still operates in resonance when misaligned. The inverter efficiency is 93.2% and the rectifier is 98.4% when the system is aligned.

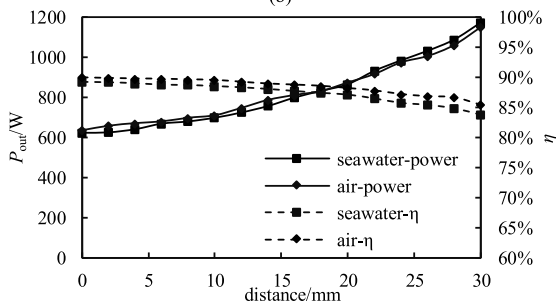
The system performance on the output power and the DC-DC efficiency over different misalignments are shown in Fig. 23. As shown in Fig. 23(a), the system delivers 633.37 Watts at a DC-DC efficiency of 89.67% in seawater and delivers 634Watts from DC to DC at an efficiency of 89.9% in air, when the system is fully aligned. The power loss distribution under water is shown in Fig. 23(b). Fig. 23(c) and Fig. 23(d) show that the differences between the air and seawater are minor at the resonance frequency of 50kHz. The maximum difference in power transfer and efficiency between air and seawater are 31.6Watts and 1.7%, separately.



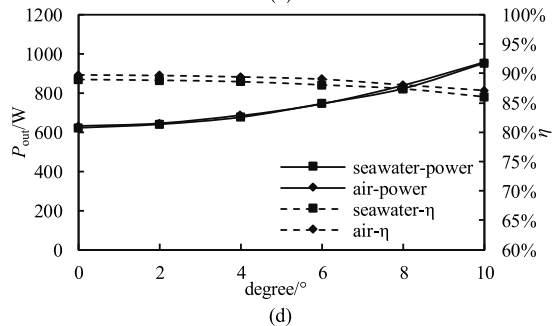
(a)



(b)



(c)



(d)

FIGURE 23. Wireless charging prototype performance in seawater and air. (a) Measured system parameters. (b) Power loss distribution. (c) Variation of P_{out} and η with axial misalignments. (d) Variation of P_{out} and η with rotational misalignments.

As axial misalignment increases from 0mm to 30mm, the output power increases from 630Watts to 1150Watts and the efficiency drops to 85.37%. The increase of P_{out} is mainly dependent on the decrease of M and the relationship between

P_{out} and M has been shown in (8). As can be seen from the experimental results, the wireless charging system with the proposed magnetic coupler is more immune to rotational misalignment than the axial misalignment. The output power at the maximum rotational misalignment increases to 950Watts and efficiency at 87.08%.

VI. CONCLUSION

The limits of annular magnetic coupler include the weight, the coupling manner and application. In this paper, a 120mm × 35mm × 6mm dipole-coil-based magnetic coupler is applied for the AUV underwater wireless charging system. The simulation results in ANSYS Maxwell show the circumferential coupled flux linkage has a constrained magnetic field distribution under the electronics and the magnetic flux density is lower than 27μT in the vicinity of electronics. The dimensions are optimized to meet the requirements and the receiver weight is greatly reduced to 137g. Fe-based nanocrystalline soft magnetic material is used to implement the magnetic coupler, and the M and k of the nanocrystalline material are both similar to the ferrite material. The experimental prototype is built and the system transmits 630Watts in both underwater and air with the efficiency at 89.7% and 89.9%, separately.

REFERENCES

- [1] N. Tesla, "Apparatus for transmitting electrical energy," U.S. Patent 1 119 732A, Dec. 1, 1914.
- [2] S. Y. Hui, "Planar wireless charging technology for portable electronic products and Qi," *Proc. IEEE*, vol. 101, no. 6, pp. 1290–1301, Jun. 2013.
- [3] D. Ahn and P. Mercier, "Wireless power transfer with concurrent 200 kHz and 6.78 MHz operation in a single transmitter device," *IEEE Trans. Power Electron.*, vol. 31, no. 7, pp. 5018–5029, Jul. 2016.
- [4] C. Xiao, K. Wei, D. Cheng, and Y. Liu, "Wireless charging system considering eddy current in cardiac pacemaker shell: Theoretical modeling, experiments, and safety simulations," *IEEE Trans. Ind. Electron.*, vol. 64, no. 5, pp. 3978–3988, May 2017.
- [5] S. Raju, R. Wu, M. Chan, and C. P. Yue, "Modeling of mutual coupling between planar inductors in wireless power applications," *IEEE Trans. Power Electron.*, vol. 29, no. 1, pp. 481–490, Jan. 2014.
- [6] S. Li and C. C. Mi, "Wireless power transfer for electric vehicle applications," *IEEE J. Emerg. Sel. Topics Power Electron.*, vol. 3, no. 1, pp. 4–17, Mar. 2015.
- [7] Y. Zhang, K. Chen, F. He, Z. Zhao, T. Lu, and L. Yuan, "Closed-form oriented modeling and analysis of wireless power transfer system with constant-voltage source and load," *IEEE Trans. Power Electron.*, vol. 31, no. 5, pp. 3472–3481, May 2016.
- [8] Z.-S. Li, D.-J. Li, L. Lin, and Y. Chen, "Design considerations for electromagnetic couplers in contactless power transmission systems for deep-sea applications," *J. Zhejiang Univ. Sci. C*, vol. 11, no. 10, pp. 824–834, Oct. 2010.
- [9] M. Lin, D. Li, and C. Yang, "Design of an ICPT system for battery charging applied to underwater docking systems," *Ocean. Eng.*, vol. 145, no. 4, pp. 373–381, Sep. 2017.
- [10] V. Bana, M. Kerber, G. Anderson, J. D. Rockway, and A. Phipps, "Underwater wireless power transfer for maritime applications," in *Proc. IEEE Wireless Power Transf. Conf. (WPTC)*, May 2015, pp. 1–4.
- [11] C. Fang, X. Li, Z. Xie, J. Xu, and L. Xiao, "Design and optimization of an inductively coupled power transfer system for the underwater sensors of ocean buoys," *Energies*, vol. 10, no. 1, 2017, Art. no. 84.
- [12] T. McGinnis, C. P. Henze, and K. Conroy, "Inductive power system for autonomous underwater vehicles," in *Proc. OCEANS*, Sep. 2007, pp. 1–5.
- [13] A. M. Bradley, M. D. Feezor, H. Singh, and F. Y. Sorrell, "Power systems for autonomous underwater vehicles," *IEEE J. Ocean. Eng.*, vol. 26, no. 4, pp. 526–538, Oct. 2001.

- [14] Z. He, Y. Wang, L. Ding, and X. Nie, "Research on three-dimensional omnidirectional wireless power transfer system for subsea operation," in *Proc. OCEANS-Aberdeen*, Jun. 2017, pp. 1–5.
- [15] J. Zhou, D.-J. Li, and Y. Chen, "Frequency selection of an inductive contactless power transmission system for ocean observing," *Ocean Eng.*, vol. 60, no. 1, pp. 175–185, Mar. 2013.
- [16] Z. Cheng, Y. Lei, K. Song, and C. Zhu, "Design and loss analysis of loosely coupled transformer for an underwater high-power inductive power transfer system," *IEEE Trans. Magn.*, vol. 51, no. 7, pp. 1–10, Jul. 2015.
- [17] S.-L. Wang, B.-W. Song, G.-L. Duan, and X.-Z. Du, "Study on non-contact power transmission of underwater unmanned vehicle," *Electr. Mach. Control*, vol. 18, no. 6, pp. 36–41, Jun. 2014.
- [18] T. Kan, R. Mai, P. P. Mercier, and C. C. Mi, "Design and analysis of a three phase wireless charging system for lightweight autonomous underwater vehicles," *IEEE Trans. Power Electron.*, vol. 33, no. 8, pp. 6622–6632, Aug. 2018.
- [19] T. Kan, Y. Zhang, Z. Yan, P. P. Mercier, and C. C. Mi, "A rotation-resilient wireless charging system for lightweight autonomous underwater vehicles," *IEEE Trans. Veh. Technol.*, vol. 67, no. 8, pp. 6935–6942, Aug. 2018.
- [20] Z. Yan, K. Zhang, H. Wen, and B. Song, "Research on characteristics of contactless power transmission device for autonomous underwater vehicle," in *Proc. OCEANS-Shanghai*, Apr. 2016, pp. 1–5.
- [21] Z. Yan, Y. Zhang, K. Zhang, B. Song, and C. Mi, "Underwater wireless power transfer system with a curly coil structure for AUVs," *IET Power Electron.*, vol. 12, no. 10, pp. 2559–2565, Aug. 2019.
- [22] J.-G. Shi, D.-J. Li, and C.-J. Yang, "Design and analysis of an underwater inductive coupling power transfer system for autonomous underwater vehicle docking applications," *J. Zhejiang Univ. Sci. C*, vol. 15, no. 1, pp. 51–62, Jan. 2014.
- [23] M. Budhia, G. A. Covic, and J. T. Boys, "Design and optimization of circular magnetic structures for lumped inductive power transfer systems," *IEEE Trans. Power Electron.*, vol. 26, no. 11, pp. 3096–3108, Nov. 2011.



SHUAI WU received the B.S. degree in electrical engineering and automation from Shanxi Agricultural University, Jinzhong, China, in 2017, and the M.S. degree in electrical engineering from the Harbin Institute of Technology, Weihai, China, in 2019, where he is currently pursuing the Ph.D. degree. His current research interests include wireless power transfer for autonomous underwater vehicles and unmanned aerial vehicles.



JINQUAN LIU was born in Heilongjiang, China, in 1995. He received the B.S. degree in electrical engineering and automation from Zhengzhou University, Zhengzhou, China, in 2018. He is currently pursuing the M.S. degree in electrical engineering with the Academy of New Energy, Harbin Institute of Technology (HIT), Weihai, China. His current research interests include power electronics and wireless power transfer system for unmanned aerial vehicle.



current research interests include wireless power transfer systems, power converters, and inverters.

CHUNWEI CAI (Member, IEEE) was born in Shandong, China, in 1977. He received the B.S. and M.S. degrees in control theory and control engineering from Shandong University, Jinan, China, in 2001 and 2004, respectively, and the Ph.D. degree in electrical engineering from the Harbin Institute of Technology (HIT), Harbin, China, in 2013. He has been a Lecturer with HIT, Weihai, China, since 2006, where he has also been working as an Assistant Professor, since 2014.



ZHIPENG ZHANG was born in Shanxi, China, in 1993. He received the B.S. degree in electrical engineering and automation from Yanshan University, Qinhuangdao, China, in 2016. He is currently pursuing the M.S. degree in electrical engineering with the Academy of New Energy, Harbin Institute of Technology (HIT), Weihai, China. His current research interests include power electronics and wireless power transfer system for autonomous underwater vehicles.



YANYU ZHANG was born in Jiangsu, China, in 1995. He received the B.S. degree in electrical engineering and automation from the China University of Mining and Technology, Xuzhou, China, in 2018. He is currently pursuing the M.S. degree in electrical engineering with the Academy of New Energy, Harbin Institute of Technology (HIT), Weihai, China. His current research interests include power electronics and wireless power transfer system for autonomous underwater vehicle.



LONGYUN JIANG was born in Shandong, China, in 1997. He received the B.S. degree in electrical engineering and automation from the Qingdao University of Technology, Qingdao, China, in 2019. He is currently pursuing the M.S. degree in electrical engineering with the Academy of New Energy, Harbin Institute of Technology (HIT), Weihai, China. His current research interests include power electronics and wireless power transfer system for unmanned aerial vehicle.

• • •